

Joint Optimization of Geometric and Probabilistic Constellation Shaping for OFDM-ISAC Systems

Benedikt Geiger*, Fan Liu[†], Shihang Lu[†], Andrej Rode*, Laurent Schmalen*

* Communications Engineering Lab (CEL), Karlsruhe Institute of Technology (KIT), 76187 Karlsruhe, Germany

[†] Southern University of Science and Technology, China

Email: benedikt.geiger@kit.edu

Abstract—6G communications systems are expected to integrate radar-like sensing capabilities enabling novel use cases. However, integrated sensing and communications (ISAC) introduces a trade-off between communications and sensing performance because the optimal constellations for each task differ. In this paper, we compare geometric, probabilistic and joint constellation shaping for orthogonal frequency division multiplexing (OFDM)-ISAC systems using an autoencoder (AE) framework. We first derive the constellation-dependent detection probability and propose a novel loss function to include the sensing performance in the AE framework. Our simulation results demonstrate that constellation shaping enables a dynamic trade-off between communications and sensing. Depending on whether sensing or communications performance is prioritized, geometric or probabilistic constellation shaping is preferred. Joint constellation shaping combines the advantages of geometric and probabilistic shaping, significantly outperforming legacy modulation formats.

I. INTRODUCTION

Integrated sensing and communications (ISAC) is expected to equip communications networks with a sixth sense by utilizing the orthogonal frequency division multiplexing (OFDM) communication signals for radar-like sensing. This joint design reduces hardware complexity, improves energy efficiency, and enhances reliability compared to operating two separate systems [1]–[3].

However, the choice of the modulation constellation impacts sensing & communications (S&C) performance resulting in the random-deterministic trade-off [4], [5]. In essence, a Gaussian distributed constellation maximizes the communications performance for an additive white Gaussian noise (AWGN) channel, whereas constant modulus constellations maximize sensing performance [5]. These contradicting requirements on the constellation make constellation shaping a crucial tool to balance the S&C performance in practical ISAC systems.

There are three main approaches to constellation shaping: *i)* *Geometric shaping*: optimizes the location of constellation points, assuming an equal probability of occurrence for each point. *ii)* *Probabilistic shaping*: uses conventional quadrature amplitude modulation (QAM) constellation points

but optimizes the probability distribution of these points. *iii)* *Joint shaping*: optimizes both location and probability of the constellation points. These different methods have been successfully optimized and compared for communications using an autoencoder (AE) framework [6], [7]. In these works, the communications system is modeled by differentiable blocks and the constellation points and their probabilities are treated as trainable parameters.

Recently, probabilistic shaping was investigated for ISAC to trade off mutual information against side-lobe level in the ambiguity function (AF) to balance S&C performance [8], [9]. However, the AF does not capture the detection performance in practical ISAC systems in an end-to-end manner. This raises two fundamental questions: How does the constellation affect the detection probability in practical OFDM-ISAC systems? How do different approaches to constellation shaping influence the ISAC trade-off?

In this paper, we address these research gaps by first deriving the impact of the constellation on the detection probability, and employ different constellation shaping methods to balance S&C performance in an end-to-end manner. Second, we employ a bitwise AE to optimize geometric, probabilistic, and joint constellations, maximizing the generalized mutual information (GMI) under specific detection and false alarm constraints. Finally, we validate our analytical results through simulations and compare the different approaches demonstrating that our proposed joint optimization outperforms both geometric and probabilistic constellation shaping.

II. SYSTEM MODEL

In this work, we consider a monostatic bit-interleaved coded modulation OFDM-ISAC system as illustrated in Fig. 1. To reduce computational complexity and simplify the analysis, we assume that all sub-carriers apply the same constellation, and the delays of the targets are assumed to be constant multiples of the sampling time shorter than the duration of the cyclic prefix (CP). Given that the targets are static, we focus on the transmission of single OFDM symbols and neglect velocity (Doppler) estimation.

A. ISAC Transmitter

For each sub-carrier $n \in \{0, \dots, N-1\}$ of the OFDM system, a constellation mapper encodes M bits $\mathbf{b}_n \in \{0, 1\}^M$,

This work has received funding from the German Federal Ministry of Education and Research (BMBF) within the projects Open6GHub (grant agreement 16KISK010) and KOMSENS-6G (grant agreement 16KISK123). Mr. Geiger acknowledges the Networking Grant from the Karlsruhe House of Young Scientists.

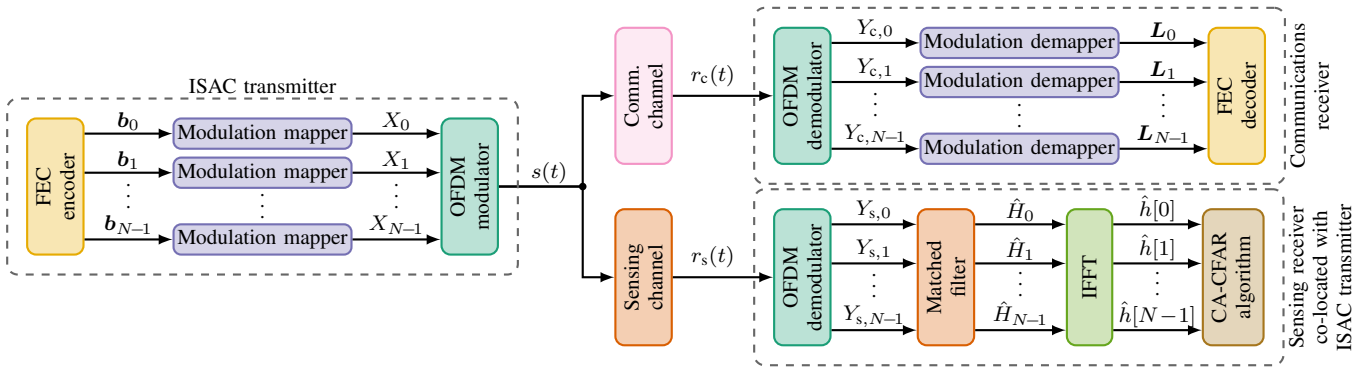


Fig. 1. Block diagram of the considered monostatic bit-interleaved coded modulation OFDM-ISAC system

obtained from a binary forward error correction (FEC) encoder, onto one of $\tilde{M} = 2^M$ modulation symbols X in the modulation alphabet \mathcal{X} , i.e., $X \in \mathcal{X} \subset \mathbb{C}$, where $|\mathcal{X}| = \tilde{M}$. Since the constellation symbols are randomly selected, the transmit symbols X_n can be considered as i.i.d. random variables (RVs) $X_n \sim P(X)$ with RVs being denoted by sans-serif font.

The OFDM modulator then transforms the N frequency domain symbols X_n , into the time domain using the orthonormal inverse fast Fourier transform (IFFT). Next, a CP is added before the baseband signal $s(t)$ is upconverted to the carrier frequency and transmitted.

B. Sensing Channel and Receiver

The arbitrary but fixed sensing channel $h(t)$ is modeled assuming J static point targets, each with a delay τ_j and a complex amplitude a_j . The received sensing signal is

$$r_s(t) = h(t) * s(t) + w_s(t) = \sum_{j=1}^J a_j s(t - \tau_j) + w_s(t), \quad (1)$$

where $w_s(t) \sim \mathcal{CN}(0, \sigma_s^2)$ denotes AWGN with variance σ_s^2 . The sensing receiver samples the baseband signal $r_s(t)$, removes the CP, and transforms it into the frequency domain using the orthonormal fast Fourier transform (FFT). The frequency domain received symbols can then be expressed as

$$Y_{s,n} = X_n H_n + W_{s,n} = X_n \frac{1}{\sqrt{N}} \sum_{j=1}^J a_j e^{-j2\pi \frac{n}{N} \tau_j} + W_{s,n}, \quad (2)$$

where H_n denotes the channel transfer function and $W_{s,n}$ is the FFT of the sampled AWGN $w_s(t)$, which follows $\mathcal{CN}(0, \sigma_s^2)$.

The sensing receiver applies a sensing matched filter (MF)

$$\hat{H}_n = Y_{s,n} X_n^* = (H_n X_n + W_{s,n}) X_n^* = H_n |X_n|^2 + W_{s,n} X_n^*, \quad (3)$$

which is an unbiased estimate of the sensing channel for unit power constellations $\mathbb{E}_X\{|X_n|^2\} = 1$

$$\mathbb{E}_X\{\hat{H}_n\} = \mathbb{E}_X\{H_n |X_n|^2\} + \mathbb{E}_X\{W_{s,n} X_n^*\} = H_n. \quad (4)$$

The delay domain channel estimate $\hat{h}[k]$ is obtained by applying the orthonormal IFFT to the frequency domain channel estimate \hat{H}_n

$$\hat{h}[k] = \frac{1}{\sqrt{N}} \sum_{n=0}^{N-1} \hat{H}_n e^{j2\pi \frac{n}{N} k}, \quad k = 0, \dots, N-1. \quad (5)$$

Finally, the cell-averaging (CA)-constant false alarm rate (CFAR) algorithm, which maximizes the detection probability P_D given a maximum false alarm rate P_{FA} , determines whether a target is present at a delay k [10].

C. Communications Channel and Receiver

For communications, the influence of a potential multipath communications channel is assumed to be suppressed by classical equalization methods and the channel is modeled as an AWGN channel with noise variance σ_c^2 , represented by $r_c(t) = s(t) + w_c(t)$, where $w_c(t) \sim \mathcal{CN}(0, \sigma_c^2)$. Similarly to the sensing receiver, the communications receiver removes the CP from the baseband signal $r_c(t)$ and converts it into the frequency domain using an orthonormal IFFT. This simplifies the OFDM system into a set of N parallel AWGN channels, one for each sub-carrier. The received communications symbol of the n th sub-carrier after equalization can therefore be modeled as

$$Y_{c,n} = X_n + W_{c,n}, \quad (6)$$

where $W_{c,n} \sim \mathcal{CN}(0, \sigma_{c,n}^2)$ is AWGN with variance $\sigma_{c,n}^2$.

The constellation demapper computes the log-likelihood ratios (LLRs) for each bit [11]

$$L_{n,m} = \log \frac{\sum_{X_n \in \mathcal{X}_m^0} f_{Y_{c,n}|X_n}(Y_{c,n}|X_n)}{\sum_{X_n \in \mathcal{X}_m^1} f_{Y_{c,n}|X_n}(Y_{c,n}|X_n)}, \quad m = 1, \dots, M, \quad (7)$$

where \mathcal{X}_m^b represents the set of constellation symbols labeled with bit $b \in \{0, 1\}$ at bit position m and $f_{Y_{c,n}|X_n}$ denotes the communications channel transition probability density function. The LLRs are a measure of the reliability of each bit, where a large magnitude indicates high reliability and a small magnitude indicates low reliability. These LLRs are eventually fed to a soft decision (SD)-FEC decoder.

To evaluate the communications performance, we use the GMI, which is a performance measure for the achievable

information rate (AIR) in practical bit-interleaved coded modulation systems [11]

$$\text{GMI}_n = \sum_{m=1}^M I(\mathbf{b}_{n,m}; \mathbf{L}_{n,m}), \quad (8)$$

where $I(\mathbf{b}_{n,m}; \mathbf{L}_{n,m})$ denotes the bitwise mutual information between the m th bit and corresponding LLR of the n th sub-carrier.

D. The Constellation-dependent Detection Probability

Since estimating the detection probability P_D using Monte Carlo simulations results in high computational complexity, we derive the constellation-dependent detection probability by analyzing each signal processing block of the sensing receiver. For the CA-CFAR algorithm, the detection probability

$$P_D = P_{\text{FA}}^{\frac{1}{1+\gamma}}, \quad (9)$$

assuming Gaussian distributed noise and interference [10] depends only on the false alarm rate P_{FA} and the average signal-to-interference-and-noise ratio (SINR) γ of the signal fed to the detection algorithm. Since the false alarm rate P_{FA} is usually fixed during system design, increasing the detection probability P_D requires increasing the average SINR γ at the input of the CA-CFAR, i.e., at the output of the IFFT.

However, when random constellation symbols are transmitted, the noise at the output of the MF, i.e., at the input of the IFFT, may no longer be Gaussian as can be observed from (3). To show that the noise is still approximately Gaussian at the output of the IFFT, we decompose the channel transfer function estimate \hat{H}_n into a deterministic part H_n and a random part \tilde{W}_n , which accounts for AWGN and the randomness of the modulation, i.e. $\hat{H}_n = H_n + \tilde{W}_n$.

For the random part \tilde{W}_n , the IFFT acts as a summation of N independent and scaled RVs \tilde{W}_n . According to the central limit theorem, the random part of the channel estimate $\tilde{w}[k] = \hat{h}[k] - h[k]$, which is the IFFT of \tilde{W}_n approximates a Gaussian if the number of sub-carriers N is sufficiently large. Fig. 2 shows the probability distribution of $\text{Re}\{\tilde{w}[k]\}$ for an increasing number of sub-carriers, demonstrating that already 64 sub-carriers are sufficient for the Gaussian assumption. This justifies modeling the detection probability using (9).

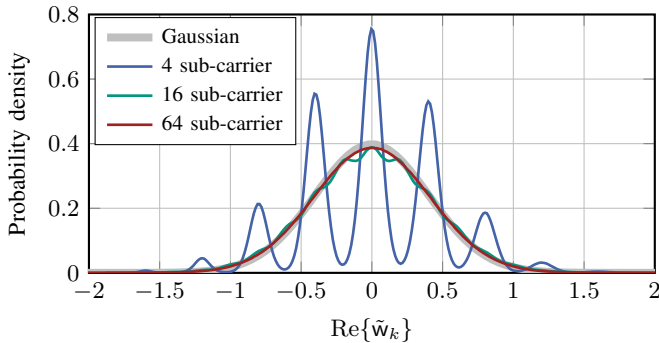


Fig. 2. Probability distribution of the noise at the input of the target detector, i.e., at the output of the IFFT assuming a 16-QAM and a sensing SNR of 20 dB in a single target scenario for various numbers of sub-carriers.

The variance

$$\sigma_{\hat{h}[k]}^2 = \left(\frac{1}{\sqrt{N}}\right)^2 \sum_{n=0}^{N-1} \sigma_{\hat{H}_n}^2 = \frac{1}{N} N \sigma_{\hat{H}_n}^2 = \sigma_{\hat{H}_n}^2 \quad (10)$$

of the delay domain channel estimate equals the variance of the frequency domain channel estimate. For the deterministic part of the channel estimate, the IFFT leads to an integration gain, increasing the power of the targets and consequently the SINR by a factor of N , as

$$\frac{1}{\sqrt{N}} \sum_{n=0}^{N-1} \sum_{j=1}^J a_j e^{-j2\pi \frac{n\tau_j}{N}} e^{j2\pi \frac{nk}{N}} = \begin{cases} \sqrt{N} a_j, & k = \tau_j \\ 0 & k \neq \tau_j. \end{cases} \quad (11)$$

Therefore, the average SINR and consequently the detection probability P_D is increased by reducing the variance

$$\begin{aligned} \sigma_{\hat{H}_n}^2 &= \mathbb{E}_{\mathbf{X}}\{|\hat{H}_n|^2\} - |\mathbb{E}_{\mathbf{X}}\{\hat{H}_n\}|^2 \\ &= |H_n|^2 (\mathbb{E}_{\mathbf{X}}\{|\mathbf{X}|^4\} - 1) + \sigma_s^2 \\ &= |H_n|^2 (\kappa - 1) + \sigma_s^2, \end{aligned} \quad (12)$$

where κ is the kurtosis of the constellation, which is equivalent to the 4th-order moment for unit power zero mean constellations. Note that unit modulus constellations like phase shift keying (PSK) have the lowest kurtosis of $\kappa = 1$, leading to the highest detection probability. A circular complex Gaussian distribution, which maximizes the AIR for an AWGN channel, has a kurtosis of $\kappa = 2$ and results in a lower detection probability [12]. From (11) and (12) follows the average SINR

$$\gamma_{\text{TOI}} = \frac{N \cdot |a_{\text{TOI}}|^2}{\sum_{j=1}^J |a_j|^2 (\kappa - 1) + \sigma_s^2}. \quad (13)$$

of a target of interest (TOI) with complex amplitude a_{TOI} at the input of the CFAR. Inserting (13) into (9) yields the constellation-dependent detection probability. We observe that the detection probability P_D depends only on the kurtosis κ of the constellation for a given scenario.

E. Optimization Problem

We aim to find the constellation that maximizes the GMI of the overall ISAC system, subject to a minimum detection probability constraint α_D , i.e. $P_D \geq \alpha_D$. Since all sub-carriers use the same constellation, the total GMI is maximized if the GMI per sub-carrier is maximized. Further, we reformulate the detection probability constraint α_D as a kurtosis constraint $\tilde{\kappa}$, i.e., $\kappa \leq \tilde{\kappa}$, because P_D depends only on the kurtosis κ of the constellation. This reduces the computational complexity and leads to the following stochastic optimization problem

$$\max_{\mathcal{X}, P(\mathbf{X})} \sum_{m=1}^M I(\mathbf{b}_m; \mathbf{L}_m) \quad (14)$$

$$\text{s.t. } \kappa \leq \tilde{\kappa} \quad (C1)$$

$$\mathbb{E}_{\mathbf{X}}\{|\mathbf{X}|^2\} = 1 \quad (C2)$$

$$\sum_{\mathbf{X}} P(\mathbf{X}) = 1 \quad (C3)$$

$$P(\mathbf{X}) \geq 0, \quad \forall \mathbf{X} \in \mathcal{X}. \quad (C4)$$

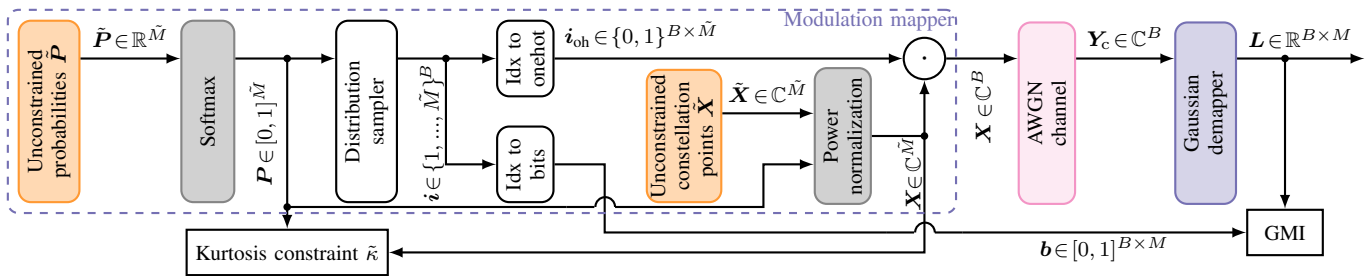


Fig. 3. Proposed AE framework to shape constellations for ISAC. The trainable parameters are marked in orange and their normalization in gray.

Here, constraint (C2) ensures that the constellation has unit power, while the constraints (C3) and (C4) enforce that $P(x)$ satisfies the properties of a probability mass function.

III. CONSTELLATION SHAPING USING AUTOENCODERS

In this section, we propose a bitwise AE framework that incorporates the sensing constraint (C1), enabling the joint optimization of both geometric and probabilistic shaping for S&C, as illustrated in Fig. 3. The AE concept enables end-to-end numerical optimization of communication systems. In our setup, the receiver is a Gaussian demapper and only the constellation of the transmitter is trainable. Depending on the shaping method (geometric, probabilistic, or joint), we optimize the constellation points, their probabilities, or both. These trainable parameters, shown as orange blocks in Fig. 3, are implemented as linear layers without bias. For more details on AE-based constellation optimization, we like to refer the reader to previous works [6], [7], [13].

For a batch size B , the distribution sampler generates random indices $i \in \{1, \dots, \tilde{M}\}^B$ according to the input distribution $P(x) \triangleq \mathbf{P}$. To ease optimization, we use the Gumbel-softmax trick and optimize the unconstrained probabilities $\tilde{\mathbf{P}} \in \mathbb{R}^{\tilde{M}}$ which are passed through a softmax layer to ensure that \mathbf{P} satisfies the probability distribution properties (C2) and (C3) [6].

These indices are then mapped to bits \mathbf{b} and one-hot vectors \mathbf{i}_{oh} . To select the transmit symbols, the one-hot vectors are pointwise multiplied with the normalized constellation points \mathbf{X} . Similar to the probabilities, we optimize the unconstrained constellation points $\tilde{\mathbf{X}}$, which are passed through a power normalization layer to obtain the unit power constellation points $\mathbf{X} \triangleq \mathbf{X}$.

The selected constellation symbols are then transmitted over an AWGN channel (6) and the LLRs (7) are computed for each bit using a classical Gaussian demapper [11]. Finally, the GMI (8), which should be maximized, is computed from the bits and LLRs.

We showed in Sec. II that the detection probability constraint can be reformulated as a kurtosis constraint (C1). Therefore, we propose a sensing loss term that depends on the kurtosis of the constellation κ to satisfy the detection probability constraint

$$\mathcal{L}_{\text{sens}} = \begin{cases} 0, & \kappa \leq \tilde{\kappa} \\ d(\kappa - \tilde{\kappa}), & \kappa > \tilde{\kappa}. \end{cases} \quad (15)$$

The penalty factor $d \in \mathbb{R}^+$ controls the strength of the penalty if the kurtosis threshold $\tilde{\kappa}$ is violated. To maximize the integration gain, the overall loss function combines both S&C performance

$$\mathcal{L} = \underbrace{\frac{M - \text{GMI}}{M}}_{\text{Communications}} + \mathcal{L}_{\text{sens}}. \quad (16)$$

Note that this loss function does not strictly enforce the sensing constraint. However, the communications loss term is normalized between $[0, 1]$ and by selecting the penalty factor d sufficiently large, the sensing loss term dominates if the kurtosis constraint is violated, effectively enforcing the sensing constraint.

IV. SIMULATION RESULTS

In this section, we validate our derivation of the constellation-dependent detection probability through simulations and compare the three constellation shaping methods in terms of their S&C performance, as well as the resulting trade-off. Throughout this section, we optimize constellations with $M = 6$ bit/symbol for each kurtosis constraint $\tilde{\kappa} \in [1, 2]$ independently, under a communications SNR of $\text{SNR}_c = 10$ dB and a penalty factor $d = 3$. The constellations are initialized as QAM and optimized by minimizing the loss function (16) using the Adam optimizer. During training, we increase the batch size increases from 500 to 10,000, while we decrease the learning rate, with the initial value depending on the shaping method. As discussed in Sec. II, the strongest sensing constraint $\tilde{\kappa} = 1$ should maximize sensing performance. On the contrary, a larger kurtosis constraint $\tilde{\kappa}$ is expected to improve communications performance, which is maximized for a circular symmetric Gaussian, that has a kurtosis of $\kappa = 2$. A kurtosis constraint $\tilde{\kappa}$ between these two extremes should yield a trade-off between S&C performance.

A. Optimized Constellations

Fig. 4 shows the optimized constellations using geometric, probabilistic and joint constellation shaping for three kurtosis constraints $\tilde{\kappa}$. We note that the strongest sensing constraint $\tilde{\kappa} = 1.0$ results in unit modulus constellations to reduce the sensing loss term (15). In this case, both geometrically and jointly shaped constellations resemble a PSK with overlapping constellation points. For probabilistic constellation shaping, a PSK is only approximated because the constellation points which have the same power do

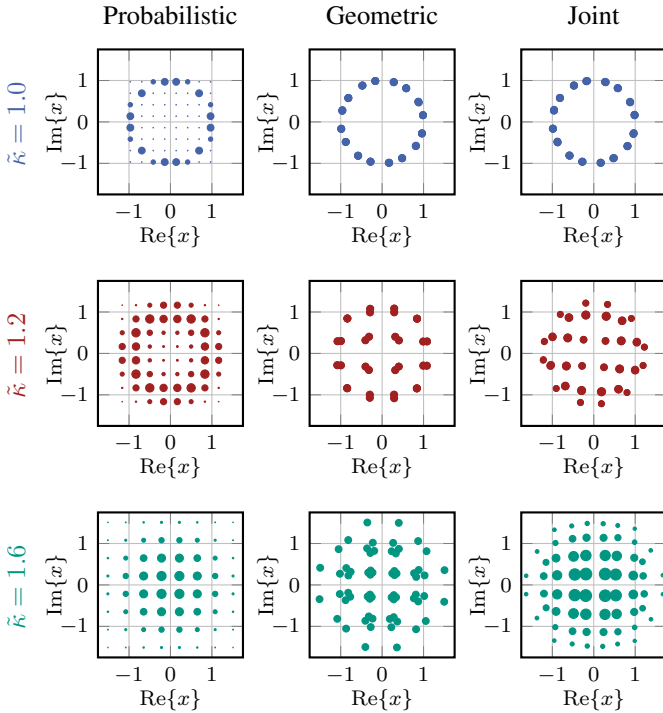


Fig. 4. Optimized constellations for geometric, probabilistic and joint constellation shaping under various kurtosis constraints $\tilde{\kappa}$. The size of each constellation point is proportional to its probability and each constellation point has an associated bit label, which is omitted for clarity.

not have equal distances. For a loose sensing constraint, the constellations approximate a Gaussian distribution to maximize communications performance. Between these two extremes ($\tilde{\kappa} = 1.2$), a balance between Gaussian and unit modulus distribution is learned depending on the kurtosis constraint $\tilde{\kappa}$. Interestingly, the jointly shaped constellations exhibit more geometric shaping characteristics for a small kurtosis constraint $\tilde{\kappa}$ and more probabilistic behavior as the kurtosis constraint $\tilde{\kappa}$ increases.

B. Sensing Performance

In Fig. 5, we consider a scenario with two targets: a distant interfering target and a nearby TOI, which should be detected and whose distance is varied. Multi-target scenarios are of particular interest because the average SINR (13) depends on the kurtosis and the power reflected by all targets. The simulation setup follows [14], with the simulation parameters being the FR2 case from [15] with only one OFDM symbol. For the CA-CFAR, we assume a false alarm rate of $P_{FA} = 10^{-3}$ and a sliding window length of $N = 100$.

We found that the simulated detection probabilities (markers) align well with the analytical constellation-dependent detection probabilities (curves), verifying our derivation in Sec. II. The minor discrepancies stem from the fact that the kurtosis κ of the optimized constellations does not exactly match the kurtosis constraint $\tilde{\kappa}$. As expected from (9) and (13), the detection probability decreases with increasing kurtosis κ and depends only on the kurtosis of the constellation, irrespective of the specific shaping method. Moreover, our

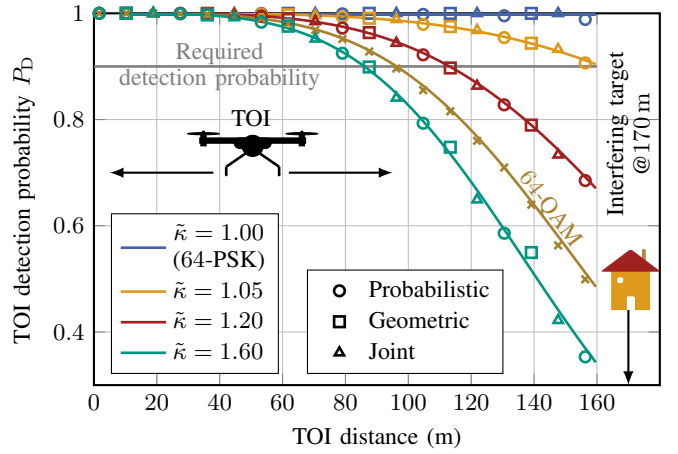


Fig. 5. Derived and simulated detection probability of a TOI, e.g. a drone, with an RCS of $\sigma_{RCS} = 0.1 \text{ m}^2$ following a Swerling-1 model in the presence of an interfering target, e.g. a building, at 170 m with an RCS of $\sigma_{RCS} = 500 \text{ m}^2$ following a Swerling-0 model [10].

simulations demonstrate that constellation shaping enables a dynamic adjustment of the detection range. For example, for a required detection probability of $P_D = 0.9$, the detection range can be varied from 90 m to beyond 160 m by modifying the kurtosis κ of the constellation.

C. Communications Performance

Fig. 6 shows the GMI as a function of the communications SNR for various sensing constraints $\tilde{\kappa}$. For $\tilde{\kappa} = 2$, all shaping methods reduce the gap to capacity and outperform the conventional 64-QAM across an SNR range of 10 dB. For large SNR values, the GMI of the probabilistically and jointly shaped constellations plateaus below 6 bit/symbol, since the constellations are optimized for a communications SNR of $\text{SNR}_c = 10 \text{ dB}$ resulting in constellations with lower entropy and, consequently, a lower maximum GMI. For $\tilde{\kappa} = 1$, the GMI of the shaped constellations is similar to that of the PSK, although probabilistic constellation shaping performs slightly worse due to unequal distances between the constellation points and the absence of Gray coding. Both geometric and joint constellations outperform the 64-PSK because their

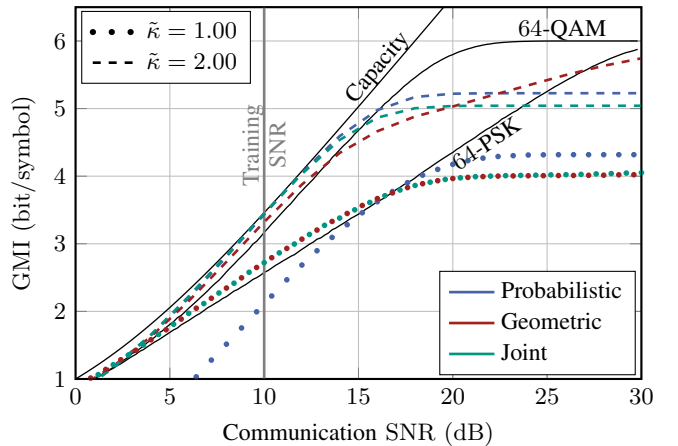


Fig. 6. Simulated communications performance (AIR) of the optimized constellations in comparison to legacy constellation formats.

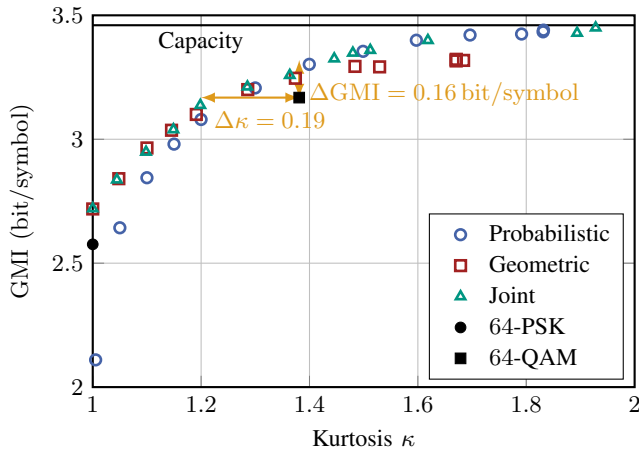


Fig. 7. Comparison of the S&C trade-off between the shaping methods. Joint constellation achieves the performance of the superior shaping method for all kurtosis constraints.

resulting constellations resemble a 16-PSK which achieves a higher GMI at low SNR values.

D. Communications-sensing Trade-off

Finally, Fig. 7 shows the GMI as a function of the kurtosis κ for the three constellation shaping methods, which effectively illustrates the communications-sensing (random-deterministic) trade-off. We note that a higher GMI can be achieved given a larger kurtosis κ , with a particularly steep improvement at lower kurtosis values. Even without a kurtosis constraint $\bar{\kappa}$, the kurtosis κ of the optimized constellation saturates below $\kappa = 2$ due to the low maximum amplitude of the optimized constellations compared to a Gaussian having infinitely extended tails.

We observe that probabilistic constellation shaping effectively approaches the capacity and outperforms geometric constellation shaping if the sensing constraint is loose. On the contrary, geometric constellation shaping outperforms probabilistic constellation shaping for strict sensing constraints $\bar{\kappa} < 1.3$. This makes geometric and probabilistic constellation shaping well-suited for applications where sensing or communications performance is prioritized, respectively.

Remark: Joint constellation shaping combines the strengths of both approaches, maximizing the integration gain. It performs similarly to geometric and probabilistic constellation shaping at low and high kurtosis values, respectively. Compared to a conventional 64-QAM, joint constellation shaping increases the GMI by 0.16 bit/symbol and reduces the kurtosis κ by 0.19 while maintaining an equivalent S&C performance. Additionally, while 64-PSK and 64-QAM offer only two discrete operating points, joint constellation shaping allows for continuous adjustment between S&C performance, providing greater flexibility. This makes joint constellation shaping a promising candidate for future 6G mobile communications systems, where maximizing performance and delivering a flexible trade-off between S&C capabilities will be crucial.

V. CONCLUSION

In this work, we employed an AE framework to optimize geometric, probabilistic, and joint constellation shaping to improve S&C performance simultaneously. We derived that the detection probability depends only on the kurtosis of the constellation and is therefore independent of the applied shaping technique. Our simulations demonstrate that geometric shaping achieves a higher GMI under strict sensing constraints, while probabilistic shaping performs better under relaxed sensing constraints. Notably, our proposed joint shaping approach combines the strengths of both geometric and probabilistic constellation shaping, significantly outperforming legacy constellation formats. This makes joint constellation shaping a promising candidate for 6G ISAC systems, which need to deliver S&C capabilities efficiently and dynamically.

REFERENCES

- [1] T. Wild, A. Grudnitsky, S. Mandelli, M. Henninger, J. Guan, and F. Schaich, "6G integrated sensing and communication: From vision to realization," in *Proc. European Radar Conference (EuRAD)*, Berlin, Germany, Sep. 2023, pp. 355–358.
- [2] F. Liu, Y. Cui, C. Masouros, J. Xu, T. X. Han, Y. C. Eldar, and S. Buzzi, "Integrated sensing and communications: Toward dual-functional wireless networks for 6G and beyond," *IEEE J. Sel. Areas Commun.*, vol. 40, no. 6, pp. 1728–1767, Jun. 2022.
- [3] S. Lu *et al.*, "Integrated sensing and communications: Recent advances and ten open challenges," *IEEE Internet Things J.*, vol. 11, no. 11, pp. 19 094–19 120, Jun. 2024.
- [4] M. F. Keskin, M. M. Mojahedian, C. Marcus, O. Eriksson, A. Giorgetti, J. Widmer, and H. Wymeersch, "Fundamental trade-offs in monostatic ISAC: A holistic investigation towards 6G," Aug. 2024, preprint, available at <https://arxiv.org/abs/2401.18011v2>.
- [5] Y. Xiong, F. Liu, K. Wan, W. Yuan, Y. Cui, and G. Caire, "From torch to projector: Fundamental tradeoff of integrated sensing and communications," *IEEE BITS the Information Theory Magazine*, 2024.
- [6] M. Stark, F. Ait Aoudia, and J. Hoydis, "Joint learning of geometric and probabilistic constellation shaping," in *Proc. IEEE GLOBECOM Workshops*, Waikoloa, HI, USA, Dec. 2019.
- [7] V. Aref and M. Chagnon, "End-to-end learning of joint geometric and probabilistic constellation shaping," in *Proc. Opt. Fiber Commun. Conf. (OFC)*, San Diego, CA, USA, Mar. 2022, p. W4I.3.
- [8] Z. Du, F. Liu, Y. Xiong, T. X. Han, Y. C. Eldar, and S. Jin, "Reshaping the ISAC tradeoff under OFDM signaling: A probabilistic constellation shaping approach," *IEEE Trans. Signal Process.*, 2024.
- [9] X. Yang, R. Zhang, D. Zhai, F. Liu, R. Du, and T. X. Han, "Constellation design for integrated sensing and communication with random waveforms," *IEEE Wireless Commun. Lett.*, 2024.
- [10] M. A. Richards, *Fundamentals of Radar Signal Processing*, 2nd ed. New York: McGraw-Hill Education, 2014.
- [11] M. Ivanov, C. Häger, F. Brännström, A. Graell i Amat, A. Alvarado, and E. Agrell, "On the information loss of the max-log approximation in BICM systems," *IEEE Trans. Inf. Theory*, vol. 62, no. 6, pp. 3011–3025, Jun. 2016.
- [12] F. Liu, Y. Zhang, Y. Xiong, S. Li, W. Yuan, F. Gao, S. Jin, and G. Caire, "OFDM achieves the lowest ranging sidelobe under random ISAC signaling," Jul. 2024, preprint, available at <https://arxiv.org/abs/407.06691>.
- [13] A. Rode, B. Geiger, S. Chimmalgi, and L. Schmalen, "End-to-end optimization of constellation shaping for Wiener phase noise channels with a differentiable blind phase search," *J. Lightw. Technol.*, vol. 41, no. 12, pp. 3849–3859, Jun. 2023.
- [14] M. Braun, "OFDM radar algorithms in mobile communication networks," Ph.D. dissertation, Karlsruhe Institute of Technology, 2014.
- [15] S. Mandelli, M. Henninger, M. Bauhofer, and T. Wild, "Survey on integrated sensing and communication performance modeling and use cases feasibility," in *Proc. International Conference on 6G Networking (6GNet)*, Paris, France, Oct. 2023.